Astronomy & Astrophysics

Galactic cold cores

VIII. Filament formation and evolution:
Filament properties in context with evolutionary models[*]

A. Rivera-Ingraham[1], I. Ristorcelli[2,3], M. Juvela[4], J. Montillaud[5], A. Men'shchikov[6], J. Malinen[4], V.-M. Pelkonen[5,4,7],
A. Marston[1], P. G. Martin[8], L. Pagani[9,10], R. Paladini[11], D. Paradis[2,3], N. Ysard[12], D. Ward-Thompson[13],
J.-P. Bernard[2,3], D. J. Marshall[6], L. Montier[2,3], and L. V. Tóth[14]

[1] European Space Astronomy Centre (ESA/ESAC), Operations Department, Villanueva de la Cañada (Madrid), Spain
   e-mail: alana.rivera@sciops.esa.int
[2] Université de Toulouse, UPS-OMP, IRAP, Toulouse, France
[3] CNRS, IRAP, 9 Av. colonel Roche, BP 44346, 31028 Toulouse Cedex 4, France
[4] Department of Physics, PO Box 64, 00014 University of Helsinki, Finland
[5] Institut UTINAM, CNRS 6213, OSU THETA, Université de Franche-Comté, 41bis avenue de l'Observatoire, 25000 Besançon,
   France
[6] Laboratoire AIM, CEA/DSM/Irfu – CNRS/INSU – Université Paris Diderot, CEA-Saclay, 91191 Gif-sur-Yvette Cedex, France
[7] Finnish Centre for Astronomy with ESO, University of Turku, Väisäläntie 20, 21500 Piikkiö, Finland
[8] Canadian Institute for Theoretical Astrophysics, University of Toronto, 60 St. George Street, Toronto, ON M5S 3H8, Canada
[9] LERMA, Observatoire de Paris, PSL Research University, CNRS, UMR 8112, 75014 Paris, France
[10] Sorbonne Universités, UPMC Univ. Paris 6, UMR 8112, LERMA, 75005 Paris, France
[11] Infrared Processing Analysis Center, California Institute of Technology, 770 S. Wilson Ave., Pasadena, CA 91125, USA
[12] IAS, CNRS (UMR8617), Université Paris Sud, Bât. 121, 91400 Orsay, France
[13] Jeremiah Horrocks Institute, University of Central Lancashire, Preston, Lancashire, PR1 2HE, UK
[14] Eötvös University, Department of Astronomy, Pázmány P. s. 1/a, 1117 Budapest, Hungary

ABSTRACT

Context. The onset of star formation is intimately linked with the presence of massive unstable filamentary structures. These filaments are therefore key for theoretical models that aim to reproduce the observed characteristics of the star formation process in the Galaxy.
Aims. As part of the filament study carried out by the *Herschel* Galactic Cold Cores Key Programme, here we study and discuss the filament properties presented in GCC VII (Paper I) in context with theoretical models of filament formation and evolution.
Methods. A conservatively selected sample of filaments located at a distance $D < 500\,$pc was extracted from the GCC fields with the *getfilaments* algorithm. The physical structure of the filaments was quantified according to two main components: the central (Gaussian) region of the filament (core component), and the power-law-like region dominating the filament column density profile at larger radii (wing component). The properties and behaviour of these components relative to the total linear mass density of the filament and the column density of its environment were compared with the predictions from theoretical models describing the evolution of filaments under gravity-dominated conditions.
Results. The feasibility of a transition from a subcritical to supercritical state by accretion at any given time is dependent on the combined effect of filament intrinsic properties and environmental conditions. Reasonably self-gravitating (high $M_{\rm line,core}$) filaments in dense environments ($A_{\rm V} \gtrsim 3\,$mag) can become supercritical on timescales of $t \sim 1\,$Myr by accreting mass at constant or decreasing width. The trend of increasing $M_{\rm line,tot}$ ($M_{\rm line,core}$ and $M_{\rm line,wing}$) and ridge $A_{\rm V}$ with background for the filament population also indicates that the precursors of star-forming filaments evolve coevally with their environment. The simultaneous increase of environment and filament $A_{\rm V}$ explains the observed association between dense environments and high $M_{\rm line,core}$ values, and it argues against filaments remaining in constant single-pressure equilibrium states. The simultaneous growth of filament and background in locations with efficient mass assembly, predicted in numerical models of filaments in collapsing clouds, presents a suitable scenario for the fulfillment of the combined filament mass−environment criterium that is in quantitative agreement with *Herschel* observations.

Key words. ISM: clouds – infrared: ISM – submillimeter: ISM – dust, extinction – stars: formation

1. Introduction

Filamentary structures are a wide-spread phenomenon in the interstellar medium (ISM). They constitute a complex hierarchical population with a wide range of properties in terms of crest (ridge) column density, linear mass density ($M_{\rm line}$), and length (e.g. Hacar et al. 2013; Hennemann et al. 2012). Observations carried out with the *Herschel* Space Observatory (*Herschel*; Pilbratt et al. 2010) indicate that filaments in the local neighbourhood might be characterised by a quasi-constant average width of ~0.1 pc (e.g. Arzoumanian et al. 2011), although with a wide spread around this value and possibly even increasing at larger distances (e.g. Juvela et al. 2012; Schisano et al. 2014).

---

[*] *Herschel* is an ESA space observatory with science instruments provided by European-led Principal Investigator consortia and with important participation from NASA.

Filaments are also ubiquitous in a wide range of environments and conditions, from the most diffuse regions at high galactic latitudes (e.g. Miville-Deschênes et al. 2010) to the active high-mass star forming complexes (e.g. Hennemann et al. 2012).

Despite their diversity, the observed tendency of pre-stellar cores and young stellar objects (YSOs) to be associated with the densest and most massive of these filaments (supercritical: $M_{line} > M_{crit}$, where $M_{crit} = 2c_s^2/G \sim 16.5\,M_{\odot}\,pc^{-1}$ for a dust temperature of $T \approx 10\,K$; e.g. Inutsuka & Miyama 1992; André et al. 2010) has made them a critical component that needs to be accurately constrained for the development of viable observational and theoretical models of star formation. Processes such as global cloud collapse (e.g. Peretto et al. 2013), convergence of large-scale flows (e.g. Schneider et al. 2010), or cloud-cloud collisions (e.g. Duarte-Cabral et al. 2011) are examples of the various scenarios invoked to account for the presence of filaments in star-forming regions.

Rivera-Ingraham et al. (2016; Paper I hereafter) used the data acquired by the *Herschel* Galactic Cold Cores Key Programme (GCC; PI: M. Juvela; Juvela et al. 2012) to extract a sample of filaments for Galactic fields located at $D \leq 500\,pc$. This study complemented the work presented in Juvela et al. (2012) and aimed to provide a reliable characterisation of the physical properties of the filament population under different environmental conditions. The goal of this work is to apply and interpret the results derived in Paper I in context with the predictions from gravity-dominated models of star formation. Comparison between the observed filament properties and predictions from these models will lead to a better understanding of the processes and conditions needed for the formation of star-forming filaments in (gravity-driven) scenarios. The role of external events in filament formation such as external feedback and collisions are the subject of ongoing work and will be published in an upcoming study.

This work is organised according to the following structure: in Sects. 2 and 3 we provide a brief summary of the datasets and methods used in Paper I to identify and characterise the filament sample. The key properties extracted from the filament catalogue are included in Sect. 4. These results are analysed and discussed in Sect. 5 in order to constrain the formation process of star-forming supercritical according to accretion-based models. Our conclusions are listed in Sect. 6.

2. *Herschel* maps and data processing

The *Herschel* maps with filament detections that were used in Paper I consist of a subsample of 38 fields out of the 116 regions observed by the GCC Programme (see Juvela et al. 2012; and Montillaud et al. 2015; for a detailed description of the processing and map properties).

The SPIRE ($250\,\mu m$, $350\,\mu m$, and $500\,\mu m$; Griffin et al. 2010) and PACS $160\,\mu m$ maps (Poglitsch et al. 2010) were processed with the *Herschel* Interactive Processing Environment (HIPE[1]) v.10.0 and the *Scanamorphos* package version 20 (Roussel 2013), respectively.

Column density and temperature maps were produced from the colour- and offset-corrected SPIRE brightness maps convolved to a common resolution of 40″. The pixel-by-pixel fitting of spectral energy distributions (SEDs) was carried out assuming a dust opacity of $0.1\,cm^2\,g^{-1}$ at 1 THz (Hildebrand 1983) for a fixed dust emissivity index of $\beta = 2$. We assumed a mean atomic

weight per molecule of $\mu = 2.33$ for consistency with previous filament studies.

3. Method: detection and characterisation of the filament sample

The target structures of our analysis consisted of the most robust filamentary detections located at $D < 500\,pc$ that are directly linked to the formation of cores within the resolution limitations of the data (full with at half maximum: $FWHM_{core} < 0.2\,pc$). The process of filament extraction, selection, and analysis are outlined below, and we refer to Paper I for a detailed description of the process and techniques employed.

A preliminary catalogue of filament detections in each field was obtained from the N_{H_2} maps using the *getfilaments* algorithm v1.140127 (Men'shchikov 2013). This initial extraction was carried out as part of the source-detection process performed with the multi-scale multi-wavelength source extraction algorithm *getsources* (Men'shchikov et al. 2012). During the filament detection process, *getfilaments* effectively identified and separated all the filamentary contribution in the map from the contribution associated with compact sources and background or noise fluctuations, providing a set of images with clean filament profiles from which physical parameters such as width, length, and intensity can be derived. The algorithm also quantified for each filament pixel the fraction of the total intensity associated with different spatial scales in the image. Only those filaments with significant emission in the spatial scales relevant for the formation of pre-stellar cores ($<0.2\,pc$ at $D \leq 500\,pc$) were considered to be core-bearing filaments (core-scale filaments) and were selected for further analysis.

The filament population was characterised by examining the structural and environmental properties of each filament. The average radial column density profile of each detection (including contribution from compact sources to the profile) was fitted with an idealised model of a Plummer-like (Whitworth & Ward-Thompson 2001; Nutter et al. 2008) cylindrical filament using a non-linear least-squares minimisation routine. Integration of the best-fit profile yielded an estimate of the total linear mass density ($M_{line,tot}$). Following the approach used in previous studies, the filament profile was further assumed to be characterised by a Gaussian-like inner region comprising the most central and densest parts of the filament. This component was described in Paper I as the filament core-component, and it defines the characteristic *FWHM* of the filament. The wing-component is dominated by the power-law-like region of the filament profile at large radii, so that the total linear mass density can be expressed as $M_{line,tot} = M_{line,core} + M_{line,wing}$. The mean intrinsic column density of the filament was estimated by averaging the values of the pixels associated with the filament crest. An estimate of the background level was obtained by averaging the same pixels, but with N_{H_2} values measured from the complementary background map obtained by *getfilaments* (*getsources*) during the filament extraction process.

4. Results: potential evolutionary trends for accretion-based models

A total of 14 fields contained filaments in the local neighbourhood that satisfied the intrinsic and reliability criteria established for the selection of core-bearing filaments. These filaments were classified according to the component dominating their total linear mass density (core-dominated if $M_{line,core}/M_{line,wing} > 1$, wing-dominated otherwise), stability (supercritical if $M_{line,tot} \geq M_{crit}$, subcritical otherwise), and

---

Table 1. Filament parameters of the regimes for the core-scale filament sample.

Regime	$\langle M_{\text{line,core}} \rangle$ $[M_\odot \, \text{pc}^{-1}]$	$\langle M_{\text{line,wing}} \rangle$ $[M_\odot \, \text{pc}^{-1}]$	$\langle N_{\text{H}_2} \rangle^a$ $[10^{20} \, \text{cm}^{-2}]$	$\langle A_{\text{V}} \rangle^{a,b}$ [mag]	$\langle \text{BKG } N_{\text{H}_2} \rangle$ $[10^{20} \, \text{cm}^{-2}]$	$\langle \text{BKG } A_{\text{V}} \rangle^b$ [mag]	$FWHM$ [pc]
1 ALL	2.16 ± 0.22	2.40 ± 0.70	8.92 ± 0.82	0.95 ± 0.09	13.77 ± 2.05	1.46 ± 0.22	0.11 ± 0.01
1 ALL(HB)^c	2.43 ± 0.40	3.29 ± 1.98	12.34 ± 2.02	1.31 ± 0.21	26.90 ± 2.53	2.86 ± 0.27	0.09 ± 0.01
1 ALL(LB)^c	2.08 ± 0.26	2.13 ± 0.72	7.86 ± 0.69	0.84 ± 0.07	9.73 ± 1.01	1.04 ± 0.11	0.11 ± 0.01
2 ALL	5.97 ± 0.25	7.72 ± 1.38	23.02 ± 3.38	2.45 ± 0.36	25.60 ± 2.57	2.72 ± 0.27	0.14 ± 0.01
2 ALL(HB)	5.97 ± 0.27	6.47 ± 2.04	28.51 ± 5.80	3.03 ± 0.62	35.35 ± 1.48	3.76 ± 0.16	0.11 ± 0.02
2 ALL(LB)	5.96 ± 0.44	9.11 ± 1.84	16.93 ± 1.85	1.80 ± 0.20	14.77 ± 0.92	1.57 ± 0.10	0.18 ± 0.02
2 SB^d	6.10 ± 0.30	3.57 ± 0.73	21.04 ± 2.54	2.24 ± 0.27	25.36 ± 3.27	2.70 ± 0.35	0.15 ± 0.02
2 SB (HB)	5.77 ± 0.30	2.69 ± 0.83	22.80 ± 3.87	2.43 ± 0.41	33.91 ± 1.89	3.61 ± 0.20	0.13 ± 0.02
2 SB (LB)	6.58 ± 0.56	4.81 ± 1.17	18.58 ± 2.95	1.98 ± 0.31	13.40 ± 1.29	1.43 ± 0.14	0.18 ± 0.03
2 SP^d	5.73 ± 0.44	14.83 ± 0.74	26.43 ± 8.35	2.81 ± 0.89	26.01 ± 4.51	2.77 ± 0.48	0.14 ± 0.03
2 SP (HB)	6.45 ± 0.56	15.29 ± 1.47	41.85 ± 16.54	4.45 ± 1.76	38.71 ± 0.32	4.12 ± 0.03	0.08 ± 0.03
2 SP (LB)	5.20 ± 0.55	14.49 ± 0.85	14.87 ± 1.86	1.58 ± 0.20	16.48 ± 0.76	1.75 ± 0.08	0.18 ± 0.03
3 ALL	13.61 ± 1.42	20.26 ± 5.19	52.18 ± 8.12	5.55 ± 0.86	27.70 ± 4.27	2.95 ± 0.45	0.12 ± 0.01
3 ALL(HB)	15.14 ± 1.57	23.64 ± 7.28	58.16 ± 11.03	6.19 ± 1.17	32.56 ± 4.65	3.46 ± 0.49	0.13 ± 0.02
3 ALL(LB)	10.54 ± 1.18	13.51 ± 4.25	40.21 ± 6.67	4.28 ± 0.71	17.99 ± 1.64	1.91 ± 0.17	0.12 ± 0.00

Notes. $^{(a)}$ Average intrinsic (background-free) N_{H_2} of crest and standard error on the mean. $^{(b)}$ $N_{\text{H}_2} = 9.4 \times 10^{20} \, \text{cm}^{-2} \, A_{\text{V}}/\text{mag}$. $^{(c)}$ HB = high background; LB = low background. $^{(d)}$ SB = subcritical; SP = supercritical.

environmental level (low-background (LB) filaments when the background level is below the mean of the population of $A_{\text{V}} \approx 2.2$ mag, high-background (HB) filaments when above this value[2]). We used these classifications to identify not only global properties of the filament population, but also potential trends and correlations that could provide insight into the requirements, limitations, and nature of the physical processes driving filament formation and evolution.

Three major filament regimes are identified (see Paper I): a core-dominated subcritical regime (regime 1; $M_{\text{line,core}} < 4.2 \, M_\odot \, \text{pc}^{-1}$), a transition regime comprising a mixture of core-dominated, wing-dominated, subcritical, and supercritical filaments (regime 2; $4.2 \leq M_{\text{line,core}} \leq 8.4 \, M_\odot \, \text{pc}^{-1}$), and a regime exclusively associated with supercritical filaments (regime 3; $M_{\text{line,core}} > 8.4 \, M_\odot \, \text{pc}^{-1}$). These regimes, initially selected according to their $M_{\text{line,core}}$, show distinct average structural properties ($M_{\text{line,tot}}$, crest N_{H_2}) and environment. This can be clearly observed in the global mean properties of each regime highlighted in Paper I (Tables 3 and 4), and in more detail in Table 1 of this work.

Filament growth and mass assembly via accretion, as predicted by theoretical models and observational studies (e.g. Schisano et al. 2014), would be characterised by an increase in $M_{\text{line,tot}}$ with time. Based only on the average global characteristics of the different regimes, we were able to conclude in Paper I that both components ($M_{\text{line,core}}$ and $M_{\text{line,wing}}$) appear to increase with increasing $M_{\text{line,tot}}$ (i.e. with time), with the wing component dominating the core component at high $M_{\text{line,tot}}$ (late stages) of evolution. We were also able to infer that the most massive filament components are primarily associated with the densest environments. Our results clearly indicated that local external conditions must play a fundamental role in filament evolution.

Table 1 provides a detailed list of the average properties of the different filament groups (classified according to stability and background N_{H_2} level) within each of the three regimes. The potential changes in filament structure as a function of time ($M_{\text{line,tot}}$) and environment quantified in this table are visually illustrated in Fig. 1.

In a transition from an overall subcritical to supercritical regime, filaments are characterised by an increase in central ridge column density (e.g. Fig. 1c). This would be a natural outcome for structures undergoing collapse and substructure growth via gravitational forces, especially in dense environments where such processes would be more significant because of the availability of material. Our results also indicate a roughly constant or possibly moderate decrease in filament width with time for HB filaments (Fig. 1a), and an increase for LB filaments (Fig. 1b). These figures indicate that if there are indeed changes in width during filament evolution from a subcritical to supercritical regime, the small variations associated with such changes would explain the apparently constant value of this quantity for filaments in radically different environments and star-forming states (e.g. André et al. 2010). It would also support accretion as a major process in filament formation and evolution, as the presence of filaments with characteristic widths of ~0.1 pc has been theorised to be the result, at least in part, of accretion effects (e.g. accretion-driven turbulence and ion-neutral friction; Hennebelle & André 2013).

5. Discussion: filament evolution under gravity-dominated conditions

Accretion is necessary for filament growth and is therefore a key factor in any evolutionary model of filaments in the ISM. Accretion is predicted to play a crucial if not dominant role in any scenario of filament evolution. Theoretical modelling of gravitational infall onto molecular filaments carried out by Heitsch (2013) indicates that accretion cannot be prevented even in the presence of magnetic fields or turbulence. With timescales shorter than those of ambipolar and turbulent diffusion (Heitsch & Hartmann 2014), accretion is one of the most likely candidates for driving the pre-stellar core and star formation process.

---

[2] $N_{\text{H}_2} = 9.4 \times 10^{20} \, A_{\text{V}}/\text{mag}$; Bohlin et al. (1978).
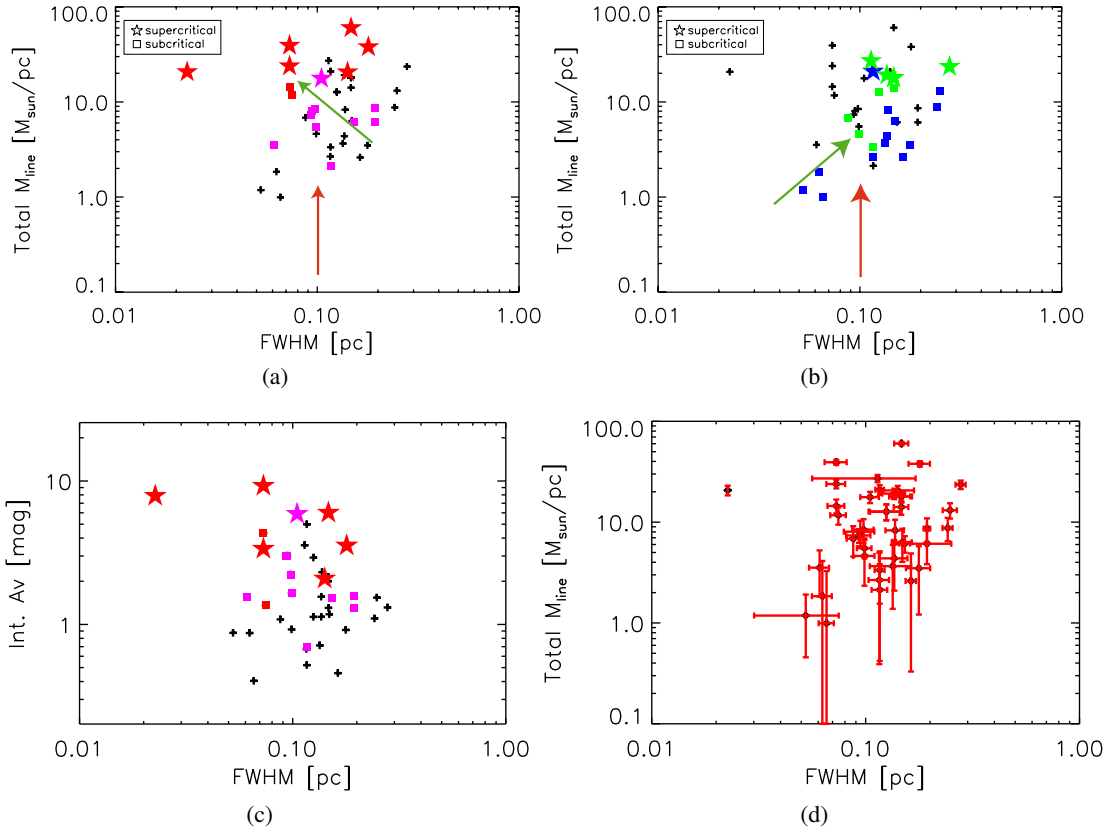
Fig. 1. Filament characteristic intrinsic total linear mass density ($M_{\mathrm{line,tot}}$) as a function of *FWHM* for HBs (filled red and magenta symbols; **a)**) and LBs (filled blue and green symbols **b)**) of the core-scale filament sample. Panel **c)** shows the $A_{\mathrm{V}} - FWHM$ distribution for HBs. As reference, black crosses in Figs. 1a and 1b mark the position of filaments in low and high backgrounds, respectively. Panel **d)** is the same as **a)** and **b)**, but with uncertainties included as reference. The red arrow indicates the evolutionary direction at constant ~0.1 pc width (e.g. Arzoumanian et al. 2011; 2013). The green arrow indicates an alternative evolutionary path leading to filaments with the same final properties and conveying similar changes as the original model, but allowing for a (conservative) change in filament width (see text). Separation according to the relative contribution of core or wing components to the filament $M_{\mathrm{line,tot}}$ is marked as follows: core dominated (blue and magenta for LBs and HBs, respectively), and wing dominated (green and red).

Evidence of mass assembly by accretion from the local environment has been readily observed for filaments associated with low- and high-mass star formation alike (e.g. Hennemann et al. 2012; Palmeirim et al. 2013). In the evolutionary model proposed in Arzoumanian et al. (2011, 2013), accreting and collapsing supercritical self-gravitating filaments would increase their linear mass density while keeping a constant filament width (~0.1 pc). An increase in linear mass density by accretion for filaments associated with the pre-stellar and proto-stellar stages of star formation was also suggested by Schisano et al. (2014) and has been observed in numerical simulations. Filaments are a general intrinsic feature of molecular clouds (Smith et al. 2016), therefore they are influenced by the evolution of their large-scale environment. Extensive periods of accretion are predicted to arise as a result of global cloud collapse (e.g. Gómez & Vázquez-Semadeni 2014; Smith et al. 2014), and the transition to a supercritical regime is an expected outcome in those regions in which the converging collapse leads to enhanced gathering of mass (Heitsch et al. 2009; Smith et al. 2016). According to simple linear mass density stability criteria, subcritical filaments are defined as gravitationally unbound and stable against collapse, therefore most likely prone to dispersion before undergoing significant star formation. It is, however, still not observationally constrained how and under which conditions subcritical filaments evolve by accretion into an unstable

supercritical regime, and how these observations fit in the proposed theoretical scenarios.

Based on their linear mass density and central crest column density, the GCC filaments comprise a key population in the intermediate region between the subcritical and supercritical states. These filaments also provide a statistically significant sample in a range of environments (e.g. Table 1). Our observations can therefore be used to constrain a possible transition process between the two states, and also the role of gravity and local environment in the formation, evolution, and the ultimate fate of filaments in the ISM.

5.1. Assumptions for a subcritical-supercritical transition process via accretion

Several scenarios have been invoked that can explain the ubiquitous presence of filaments in the ISM. These are, for instance, the resulting structures caused by large-scale gravitational collapse of clouds formed by colliding flows or streams in the ISM (e.g. Burkert & Hartmann 2004), with initial density substructure determined by turbulence and by thermal and dynamical instabilities (e.g. Heitsch et al. 2008b), and with growth aided by dynamical as well as gravitational focussing. Filaments are predicted to appear as a natural consequence of the cloud formation process (e.g. Heitsch et al. 2009). Based on these and similar

models, filament formation and evolution constitute a continuous process of which our *Herschel* observations are nothing more than snapshots in time. By definition, our observational sample comprises a set of structures with a well-developed filamentary morphology. In consequence, each of the three filament regimes (Table 1) is expected to contain filaments in different states of evolution. The use of this sample to constrain filament evolution is based on the following key results and assumptions:

1. The filament population is dominated by structures with column densities high enough for gravity to dominate (based on N_{H_2} estimates from e.g. Hartmann et al. 2001).
   The *Herschel* continuum data sets can therefore be used to broadly separate the filament sample according to their early or late evolutionary state, assuming that the general trends observed with increasing $M_{line,tot}$ for the various filament parameters (Paper I) are driven by accretion and inflow of material.

2. A supercritical filament in one regime evolves from a subcritical filament by increasing its $M_{line,tot}$ at the same time as its $M_{line,core}$, $M_{line,wing}$, and ridge N_{H_2}. These trends were observed and described in Paper I.
   Numerical simulations (e.g. Burkert & Hartmann 2004; Hartmann & Burkert 2007; Heitsch et al. 2008a; Vázquez-Semadeni et al. 2009; Smith et al. 2014; Gómez & Vázquez-Semadeni 2014) as well as observational results (e.g. Schneider et al. 2010) support the long-range effects of gravity and therefore the potentially extensive reservoir of material that can, in principle, be available for accretion. For mean infall velocities of $v \sim 0.8\,km\,s^{-1}$ (e.g. Heitsch et al. 2009) accretion of material during the predicted timescale for pre-stellar core formation and collapse can in principle occur from regions located at $\gtrsim 1$ pc from the filaments. The possibility of the environment evolving as the filament accretes implies that the precursor of a star-forming filament could be associated not only with a less massive structure, but also with a less dense background. This scenario is accounted for in our analysis by allowing filaments to evolve from a similar or more diffuse environment than that of the target supercritical structure.

3. The wing filament component dominates at a late stage of evolution.
   Our results from Paper I indicate that in a transition from subcritical to supercritical state a filament increases its $M_{line,core}$ and $M_{line,wing}$. This simultaneous growth could be compatible with that predicted for other types of structures within clouds (e.g. cores; Naranjo-Romero et al. 2015). Filaments with the highest $M_{line,tot}$ have the most massive components and are also predominantly wing dominated. A potential precursor of a star-forming filament is therefore required to be core dominated and with both $M_{line,core}$ and $M_{line,wing}$ lower than that of the target wing-dominated supercritical filament. While the actual behaviour of the filament components with time requires an extensive analysis and modelling of filament properties for a range of conditions, our choice is justified based on the general trends of the filament populations observed in Paper I and the individual properties of each regime (e.g. Table 1). In regime 2, all supercritical filaments are wing dominated and ~85% of the subcritical population is core dominated. Only two out of the six supercritical filaments in regime 3 are core dominated.

4. Mechanisms capable of providing internal support, such as turbulence or magnetic fields, do not dominate filament evolution of the global filament population.

Turbulence, for instance, is predicted to be highly linked to accretion and collapse (e.g. Burkert & Hartmann 2004), but these processes should still not be able to prevent accretion. Numerical models clearly indicate that molecular clouds are dynamically evolving and contracting gravitationally despite the presence of magnetic fields (Ibáñez-Mejía et al. 2016). The same process of large-scale global collapse drives the evolution of the internal substructure of the cloud (filament, clump), therefore gravity and mass inflow become the principal and dominant mechanisms determining changes in filamentary properties as a function of time. Observational evidence supporting the driving role of gravity is found in the shape of the observed column density probability density functions of star-forming clouds, characterised by a power-law tail at the column densities typically associated with filamentary material and star-formation (e.g. Ballesteros-Paredes et al. 2011).

By means of the above assumptions it is possible to quantify the changes associated with a transition from subcritical to supercritical state, if the filament was required to form new stars by accretion under the conditions predicted by observational and theoretical studies.

5.2. Formation and evolution of star-forming filaments

5.2.1. Preferred conditions of supercritical filaments

Supercritical (massive) filaments are found in regimes 2 ($4.2 \leq M_{line,core} \leq 8.4\,M_\odot\,pc^{-1}$) and 3 ($M_{line,core} > 8.4\,M_\odot\,pc^{-1}$), each associated with a different mean environmental column density level and filament properties (e.g. Table 1; Fig. 9 of Paper I). Figure 2 summarises the mean filament width (*FWHM*) and central ridge column density (here expressed as A_V) of supercritical filaments in each of the two regimes. As a reference, Fig. 2 also includes the predicted $FWHM-A_V$ equilibrium model for self-gravitating, accreting, and pressure-confined filaments from Fischera & Martin (2012). The theoretical curve in Fig. 2a corresponds to the default pressure used by these authors in Fig. 10 of their work, which corresponds to an environment A_V of ≈2.8 mag as estimated with Eq. (A1) of Fischera & Martin (2012). Changes on the model curve attributed to variations in external pressure (cloud environment) are highlighted Fig. 2b.

The supercritical population is most dominant in regime 3, which points towards two main requirements characterising the realm of supercritical filaments. A filament will grow, collapse, and form proto-stellar objects when it is associated with

- a moderately self-gravitating configuration with a core component already relatively close to supercritical state (e.g. a critical value for the filament ridge of $A_V \sim 5.5$ mag (background subtracted), or $M_{line,core} \gtrsim M_{crit}/2$ (Paper I); in agreement with previous studies, for example, Fischera & Martin 2012), and
- relatively dense environment ($A_V \gtrsim 3$ mag; Table 1).

Both criteria establish tight observational constraints for modelling the formation of supercritical filaments in simulations.

Interestingly, the two critical column density values (filament and environment) add to a total extinction value similar to the proposed threshold for star formation of $A_V \sim 8$ mag (e.g. André et al. 2010, 2014), which further supports a transition from subcritical to supercritical state linked to a very specific combination of filament and environmental properties. The most obvious effect arising from the fulfilment of both criteria
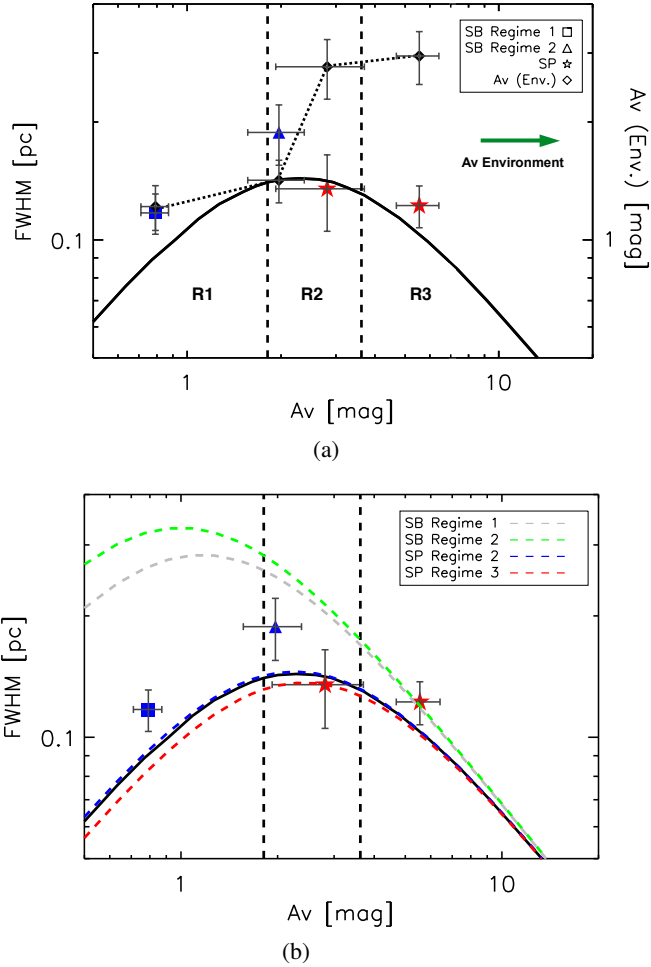
(a)

(b)

Fig. 2. Panel **a)** mean filament *FWHM* as a function of central intrinsic (crest, background subtracted) filament A_V. The black solid curve shows the model for isothermal pressure-confined filaments from Fischera & Martin (2012) for an external pressure $p_{ext}/k = 2 \times 10^4$ K cm^{-3}, i.e. environment $A_V \approx 2.8$ mag for $\mu = 2.33$. Blue and red symbols represent the average change of filament width and crest A_V for the transition from a core-dominated subcritical state (SB) to a wing-dominated supercritical state (SP). The average background for each filament group (A_V (Env.); right axis), derived from the background maps provided by *getsources* (Sect. 3), is indicated with a black symbol at the characteristic crest A_V of the group. The clear increase in environment column density with regime (crest A_V) is highlighted with a green arrow. Vertical dashed lines mark the approximate boundaries of regimes 2 and 3 for a filament with *FWHM* ≈ 0.13 pc. Boundaries would shift to lower A_V for larger *FWHM*. Error bars are the standard error on the mean for each type of filament. Panel **b)** same as panel **a)**, but highlighting the theoretical curves corresponding to the average background of each group. Models were derived using the equations included in Fischera & Martin (2012).

would be associated enhanced accretion due to the significant gravitational potential of the system and the local availability of material. The shorter build-up timescales for massive systems in dense environments (e.g. Kirk et al. 2015) would also allow the subcritical-supercritical transition to occur while fragmentation and star formation develop ($t \lesssim 1$ Myr). This scenario is consistent with the findings from Van Loo et al. (2014) and Schisano et al. (2014), who suggested that filaments initiate fragmentation while still in the formation stage. When we consider short fragmentation timescales relative to accretion (e.g. Heitsch 2013), a subcritical filament with $M_{line,core} \sim 8.5 \, M_\odot$ pc^{-1}

(maximum $M_{line,core}$ for any subcritical filament; Paper I) would quickly fragment and reach supercritical level in $\sim 10^5 - 10^6$ yr for accretion rates of $10^{-4} - 10^{-5} \, M_\odot$ pc^{-1} yr^{-1} (e.g. Schisano et al. 2014; Palmeirim et al. 2013). Taking into account the estimated lifetimes of pre-stellar cores ($\sim 10^6$ yr, e.g. André et al. 2014), our results are therefore consistent with pre-stellar substructure forming when filaments reach a significantly self-gravitating stage at $M_{line,core}$ level. This substructure would then evolve as the filament continues assembling its mass beyond the supercritical threshold, ultimately leading to the presence of accreting supercritical filaments associated with protostars and already active star formation (in agreement with results from e.g. Toalá et al. 2012).

5.2.2. Path towards supercriticality

Identification of the precursors of the supercritical filaments and their most probable evolutionary sequence depends on the assumed filament lifetime and the evolution of the filament with its environment. In Fig. 2 we have highlighted the location of subcritical filaments in regimes 1 and 2 that satisfy the criteria and our established assumptions for being potential precursors of supercritical filaments. The position of subcritical filaments in regime 1 (R1) in the figure corresponds to the mean $A_V - FWHM$ properties of filaments in this regime that have $M_{line,core}$, $M_{line,wing}$, ridge A_V, and environment A_V lower than supercritical wing-dominated filaments in regimes 2 (R2) and 3 (R3) (marked with star symbols in the diagram). Similarly, the point signalling the location of subcritical filaments in R2 traces the mean $A_V - FWHM$ properties of the core-dominated subcritical structures with linear mass densities and environmental column density below that of the wing-dominated supercritical filaments in R3.

- Filaments in regime 1 are associated predominantly with the most diffuse ($A_V \sim 1.5$ mag) environments and low central column densities barely at or below those required for reasonable self-gravitating structures (Table 1). They are also associated with the narrowest widths, which is consistent with the predictions from the (magneto-) hydrodynamical theoretical models of Hennebelle (2013).
- Subcritical filaments in regime 2 (environmental $A_V \sim 2.5$ mag) approach the turnover point of the $FWHM - A_V$ curve in Fig. 2. Filaments in these denser environments are systematically associated with higher core and wing linear mass densities (Paper I) and are therefore reasonably self-gravitating structures.

For our main assumption of a filament evolving by accretion ($M_{line,tot}$ increasing with time; e.g. Fig. 1a), the properties of filaments in the different regimes highlighted in Fig. 2 are strongly suggestive of a filament-environment co-evolutionary scenario. Filament growth, inferred by the increase in $M_{line,core}$, $M_{line,wing}$, and ridge A_V from regimes 1 to 3 appears to be intimately associated with an increase in environmental A_V, although the latter changes by a smaller degree: $\langle M_{line,core} \rangle$ and ridge $\langle A_V \rangle$ change by a factor of ~ 6, $\langle M_{line,wing} \rangle$ by ~ 8.5, and the environmental column density only increases by a factor of ~ 2 (Table 1).

Kirk et al. (2015) reported a good agreement between star-forming filaments (profiles) and the models from Fischera & Martin (2012). Likewise, the pressure-confined equilibrium model shown in Fig. 2a agrees apparently well with the supercritical filaments in this work (particularly in regime 2). A possible reason for this is that the environment A_V of these filaments is relatively similar to the environment used for that

particular model curve ($A_V \approx 2.8$ mag, cf., $\langle A_V \rangle = 2.7-2.9$ mag for regimes 2 and 3, respectively). We note that such dense environments appear to be typical of clouds with active star formation (e.g. Rivera-Ingraham et al. 2015). Subcritical filaments, on the other hand, are associated with a much lower environment A_V, which could explain their differences with respect to the equilibrium curve in Fig. 2a. We observe, however, that their properties still differ from those expected for equilibrium pressure-confined filaments in the same diffuse environments (Fig. 2b; grey and green curves). Their widths would be consistent with a much higher external pressure than the pressure predicted based on their observed environment A_V. The observed discrepancy can arise from multiple factors: different environmental temperature and chemical composition in diffuse media, inclination effects, or different mechanisms leading to out-of-equilibrium filamentary structures in diffuse environments (e.g. stellar feedback, magnetic fields, or turbulence). The local structure of many filaments in diffuse regions in the GCC sample appear to be intrinsically associated with triggered regions, such as swept-up structures and cometary globules. Furthermore, the approximation used by Fischera & Martin (2012) to derive p_{ext}/k based on environment A_V (Eq. (A1) of their work) assumes relatively dense, self-gravitating, and predominantly molecular clouds resembling pressure-confined isothermal spheres, which is an unrealistic approximation for the most diffuse fields in the GCC associated with subcritical filaments. The location and strong influence of external events on diffuse filaments therefore argue against the presence of a dominant population in equilibrium state in low-density media, with the non-self-gravitating population ultimately dispersing with time without undergoing star formation (Fig. 1b).

Despite the observed similarities with regime 2 and to some extent regime 3, the assumption of an equilibrium state for these structures is also questionable. First, structures exist with a linear mass density above the critical value for equilibrium (Eq. (4) in Fischera & Martin 2012), and filaments resolved by *Herschel* have frequently been observed to be composed of bundles of smaller scale velocity-coherent filaments (e.g. Hacar et al. 2013). Second, while equilibrium cases can well exist in non- (or slowly) evolving environments (e.g. arising from turbulent dissipation in the diffuse ISM; e.g. Tafalla & Hacar 2015), such stationary models would fail to predict a potential evolution of the filament properties with its environment as inferred from *Herschel* data for the formation of star-forming filaments.

Numerical evolutionary models in large-scale simulations provide a suitable alternative for exploring feasible scenarios consistent with observations. The simultaneous increase of environmental level with filament growth for the type of structures observed in our data is more reminiscent of the dynamically evolving filaments predicted to arise within clouds undergoing large-scale collapse. Numerical models that describe the different stages of evolution of such clouds (e.g. Gómez & Vázquez-Semadeni 2014; Kirk et al. 2015) show that filaments may evolve from a subcritical to a supercritical regime as a function of time. Furthermore, reported column density maps and animations seem to support a co-evolution of $M_{\mathrm{line,core}}$ and environment, although an actual quantification of this evolutionary process has not been reported so far, to our knowledge. Some subcritical filaments in regime 1, as well as subcritical and supercritical filaments in regime 2, can become precursors of regime 3 supercritical filaments if associated with regions of enhanced potential wells, that is, benefitting from a particularly rapid and/or continuous process of mass assembly. In numerical simulations of clouds undergoing large-scale

collapse, massive filaments with central column densities similar to those of regimes 2 and 3 are present at relatively late evolutionary stages, in the densest regions arising from the converging inflows ($t \sim 10-20$ Myr, e.g. Vázquez-Semadeni et al. 2007; Heitsch & Hartmann 2008; Gómez & Vázquez-Semadeni 2014). Once the critical filament $M_{\mathrm{line,core}}$ and environmental conditions are reached, star-formation and evolution progresses quickly as a result of the gravitational acceleration and significant mass accumulation rate associated with these conditions (e.g. Heitsch et al. 2009).

Filaments in regime 2 (Fig. 2) are associated with relatively modest star-forming potential ($\langle M_{\mathrm{line,core}} \rangle \approx 5.5 \ M_\odot \ \mathrm{pc}^{-1}$; Table 1). Taking into account the average M_{line} associated by default with star-forming filaments (M_{crit}), regime 2 supercritical filaments are more consistent with being overall quiescent structures, capable of only sporadic and isolated star-forming events. However, filaments located in growing potential wells would further benefit from a more significant, continuous, and large-scale mass-inflow, leading to a fast additional increase in $M_{\mathrm{line,tot}}$ (therefore $M_{\mathrm{line,core}}$ and $M_{\mathrm{line,wing}}$) and a transition to a fully supercritical star-forming state (regime 3) in short $t \sim 1$ Myr pre-stellar to proto-stellar transition timescales (e.g., Heitsch & Hartmann 2008; Schisano et al. 2014). The lack of publicly available models fully describing the simultaneous evolution in time of $M_{\mathrm{line,core}}$, $M_{\mathrm{line,wing}}$, filament crest A_V, width, and environmental A_V prevents a detailed comparison of these observation predictions with simulations. However, the numbers available from accretion-based models do support the interpretation of the *Herschel* data described in this work.

A well-defined filament with central crest A_V comparable to those of subcritical filaments in regime 2 is identified in the simulations from Gómez & Vázquez-Semadeni (2014) at $X, Y = 2$, -2 pc and $t = 24.4$ Myr in animation (a) Fig. 3 of that paper, for instance. Assuming a similar background as the background in regime 2 and similar dust properties in the column density calculation, this filament increases its central A_V by at least a factor of 2 by $t = 25.5$ Myr. The resulting change in A_V is remarkably similar to the change observed between supercritical filaments in regimes 2 and 3, before the filament is swept into the central regions of the cloud by the large-scale collapse of the cloud in the simulations. Within this same ~1 Myr timescale, filaments in the simulations from Smith et al. (2014) are also observed to increase their linear mass density by a factor $\gtrsim 3$, at comparable filament widths (constant or moderately decreasing – Figs. 1a, c), during their transition from subcritical to supercritical state. The trends observed in simulations under large-scale collapse are therefore in line with our observation-based predictions of a transition to supercritical state within regime 2 and extending to regime 3.

Our claim that subcritical filaments in regime 2 and even regime 1 are possible precursors of the most massive regime 3 supercritical filaments equally agrees with the same numerical models. Our chosen filament in the simulations from Gómez & Vázquez-Semadeni (2014) evolves in position and location with the inwards flow of the cloud collapse, but the filament can be traced during several Myr (animation (b)). The long-lived nature of these structures and the tendency of the environment to evolve to a denser state as a function of time with the aid of gravity (Kirk et al. 2015) allow for the filament-environment co-evolution scenario implied in Fig. 2. The similarities of the average filament properties with those expected from an equilibrium configuration would still be compatible with evolution if such a configuration is established locally by the pressure balance with the evolving environment, and on

timescales much shorter than the timescale of large-scale collapse of the region. This scenario would also explain the better agreement of equilibrium-based estimates with supercritical filaments at moderate densities, and the larger differences with the most diffuse (some likely dispersing) and the very dense (fast-evolving) structures.

A final piece of evidence in support of the large-scale gravity-driven scenario in the formation of supercritical filaments in molecular clouds is found in the filament profile change as a function of time presented in Paper I. The tendency of filaments to develop pronounced wing components ($M_{\rm line,wing}$) relative to their filament cores ($M_{\rm line,core}$) as they approach supercritical state is reminiscent of the behaviour shown by collapsing cores within a collapsing cloud in the models from Naranjo-Romero et al. (2015). A similar behaviour for the large-scale (filament) component of the core is very likely because it is an intrinsic part of the filament structure itself.

The observational model inferred by our *Herschel* observations therefore not only provides a self-consistent picture in agreement with simulations, but also agrees well with the model of dynamic star formation and the presence of a spread in stellar ages in star-forming regions (e.g. Hartmann et al. 2012; Zamora-Avilés et al. 2012). We note, however, that the fate of the filament will depend on how, where, and when the filament is formed, and not all filaments are destined to become supercritical. In a relatively constant diffuse environment (e.g. off-cloud locations, high-galactic latitudes), filaments will be quiescent and barely self-gravitating. Evolution and collapse by self-gravity of primordially low-mass filaments in these environments can be prevented by stabilising processes and by the limited accretion arising from their weak gravitational potential and the low availability of material. These structures would therefore be predominantly transient, expanding, and dispersing before the onset of star-formation. For many of these low-mass filaments, the lack of significant accretion would be consistent with the small internal velocity dispersion observed in molecular observations (Arzoumanian et al. 2013). Triggering could instead be the key driver leading to star-formation in low column density environments where gravity cannot initially play a significant role, and where wing development and accretion are therefore severely limited.

Ultimately, filament formation and evolution is a complex interplay of intrinsic and environmental conditions, most likely driven by out-of-equilibrium processes, and results from the *Herschel* data sets should be considered in context with complementary observational studies in order to develop a full model of star formation in filaments. Molecular line observations will be particularly needed to constrain the dynamical state of the filament and its environment. Such observations are critical in order to fully validate the proposed co-evolution model.

Massive supercritical filaments (and their subcritical progenitors) could also exhibit other exclusive properties not traced by our data. Our results, for instance, do not exclude the possibility of magnetic fields playing an important role in filament formation. The orientation of magnetic fields has been observed to be linked to column density (e.g. Planck Collaboration Int. XXXII 2016; Planck Collaboration Int. XXXV 2016; Malinen et al. 2016), with star-forming filaments having a preferred axis orientation with respect to the local magnetic field (e.g. André et al. 2014). Similarly, the uncertainty level of our width measurements relative to the small changes between the different regimes implies that results should be taken with caution when trying to identify a characteristic width behaviour for our (small) supercritical sample. A more significant sample of core-dominated

supercritical filaments, combined with higher resolution observations and numerical simulations, will aid in further constraining the physical conditions and timescales associated with the evolution of filaments that are already in supercritical state and are actively forming new stars.

6. Conclusions

A subsample of *Herschel* fields of the Galactic Cold Cores Programme at $D < 500$ pc has been used to investigate the observational signatures associated with the onset of star formation in filaments.

Filaments in different environments were identified and extracted with the *getfilaments* algorithm. Physical properties (linear mass density, width, and crest column density), as well as the structural components of the filament (the core innermost region and the wing power-law-like component at large radii of the filament profile) were quantified as described in Paper I. The characteristics derived from the $N_{\rm H_2}$ profile fitted with a Plummer-like function were investigated as a function of environment and stability ($M_{\rm line,tot}$). The analysis was performed in order to constrain an observation-based evolutionary model from a subcritical to a supercritical (unstable) state that can be used in context with theoretical models of filament formation and evolution.

The combination of local environment and $M_{\rm line,core}$ at a given time has a critical role in determining the evolutionary path and ultimate fate (star-forming potential) of a given filament in $t \lesssim 1$ Myr. Only strongly self-gravitating structures with a relative massive core component associated with a dense environment ($A_{\rm V} \gtrsim 3$ mag) have the potential for becoming supercritical and star-forming on timescales comparable to the observed lifetime of pre-stellar sources. Filament evolution via mass assembly progresses with little changes in filament average width ($\langle FWHM \rangle \sim 0.13$ pc). Low-mass filaments in diffuse environments tend to increase their $FWHM$ with time, while self-gravitating filaments in denser regions contract or evolve at similar width during the transition to supercriticality.

Our proposed observation-based model for the formation of supercritical star-forming filaments has been compared with predictions from numerical models of filament evolution. While filamentary properties for filaments in relatively dense media are similar to those predicted for pressure-confined filaments in equilibrium, the non-negligible differences with respect to the *Herschel* measurements and the simultaneous growth of the filament linear mass density with its environment with time implied by the *Herschel* data are more consistent with dynamical models of cloud evolution. The filament−environment coevolution scenario is an intrinsic feature of filaments in clouds undergoing large-scale collapse. Those structures formed in the potential wells that emerge during the convergent inflow motions benefit from enhanced accretion and efficient mass assembly. The physical changes of filaments during the subcritical-supercritical transition predicted by simulations are quantitatively consistent with those derived from observations.

While the average properties of a filament population can reveal clues as to their formation and evolution, the dispersion of filament properties observed in the GCC fields remains significant. Similarly, the feasibility of the evolutionary paths considered are highly dependent on the established assumptions, and the evolution itself can also be highly dependent on external conditions, such as Galactic position and physical processes forming the filament. A complete understanding of filament structure and evolution must not only investigate the effect of processes such as shocks, turbulence, and magnetic fields, together with gravity,

but the observed properties must also be considered in context with the local environment, the star-forming activity, and the history of the region. In-depth studies of these properties, even for individual fields, will be key for understanding the wide diversity of the filament population.

References

André, P., Men'shchikov, A., Bontemps, S., et al. 2010, A&A, 518, L102
André, P., Di Francesco, J., Ward-Thompson, D., et al. 2014, Protostars and Planets VI (University of Arizona Press), 27
Arzoumanian, D., André, P., Didelon, P., et al. 2011, A&A, 529, L6
Arzoumanian, D., André, P., Peretto, N., & Könyves, V. 2013, A&A, 553, A119
Ballesteros-Paredes, J., Vázquez-Semadeni, E., Gazol, A., et al. 2011, MNRAS, 416, 1436
Bohlin, R. C., Savage, B. D., & Drake, J. F. 1978, ApJ, 224, 132
Burkert, A., & Hartmann, L. 2004, ApJ, 616, 288
Duarte-Cabral, A., Dobbs, C. L., Peretto, N., & Fuller, G. A. 2011, A&A, 528, A50
Fischera, J., & Martin, P. G. 2012, A&A, 542, A77
Gómez, G. C., & Vázquez-Semadeni, E. 2014, ApJ, 791, 124
Griffin, M. J., Abergel, A., Abreu, A., et al. 2010, A&A, 518, L3
Hacar, A., Tafalla, M., Kauffmann, J., & Kovács, A. 2013, A&A, 554, A55
Hartmann, L., & Burkert, A. 2007, ApJ, 654, 988
Hartmann, L., Ballesteros-Paredes, J., & Bergin, E. A. 2001, ApJ, 562, 852
Hartmann, L., Ballesteros-Paredes, J., & Heitsch, F. 2012, MNRAS, 420, 1457
Heitsch, F. 2013, ApJ, 769, 115
Heitsch, F., & Hartmann, L. 2008, ApJ, 689, 290
Heitsch, F., & Hartmann, L. 2014, MNRAS, 443, 230
Heitsch, F., Hartmann, L. W., & Burkert, A. 2008a, ApJ, 683, 786
Heitsch, F., Hartmann, L. W., Slyz, A. D., Devriendt, J. E. G., & Burkert, A. 2008b, ApJ, 674, 316
Heitsch, F., Ballesteros-Paredes, J., & Hartmann, L. 2009, ApJ, 704, 1735
Hennebelle, P. 2013, A&A, 556, A153
Hennebelle, P., & André, P. 2013, A&A, 560, A68
Hennemann, M., Motte, F., Schneider, N., et al. 2012, A&A, 543, L3
Hildebrand, R. H. 1983, QJRAS, 24, 267
Ibáñez-Mejía, J. C., Mac Low, M.-M., Klessen, R. S., & Baczynski, C. 2016, ApJ, 824, 41
Inutsuka, S.-I., & Miyama, S. M. 1992, ApJ, 388, 392
Juvela, M., Ristorcelli, I., Pagani, L., et al. 2012, A&A, 541, A12
Kirk, H., Klassen, M., Pudritz, R., & Pillsworth, S. 2015, ApJ, 802, 75
Malinen, J., Montier, L., Montillaud, J., et al. 2016, MNRAS, 460, 1934
Men'shchikov, A. 2013, A&A, 560, A63
Men'shchikov, A., André, P., Didelon, P., et al. 2012, A&A, 542, A81
Miville-Deschênes, M.-A., Martin, P. G., Abergel, A., et al. 2010, A&A, 518, L104
Montillaud, J., Juvela, M., Rivera-Ingraham, A., et al. 2015, A&A, 584, A92
Naranjo-Romero, R., Vázquez-Semadeni, E., & Loughnane, R. M. 2015, ApJ, 814, 48
Nutter, D., Kirk, J. M., Stamatellos, D., & Ward-Thompson, D. 2008, MNRAS, 384, 755
Palmeirim, P., André, P., Kirk, J., et al. 2013, A&A, 550, A38
Peretto, N., Fuller, G. A., Duarte-Cabral, A., et al. 2013, A&A, 555, A112
Pilbratt, G. L., Riedinger, J. R., Passvogel, T., et al. 2010, A&A, 518, L1
Planck Collaboration Int. XXXII. 2016, A&A, 586, A135
Planck Collaboration Int. XXXV. 2016, A&A, 586, A138
Poglitsch, A., Waelkens, C., Geis, N., et al. 2010, A&A, 518, L2
Rivera-Ingraham, A., Martin, P. G., Polychroni, D., et al. 2015, ApJ, 809, 81
Rivera-Ingraham, A., Ristorcelli, I., Juvela, M., et al. 2016, A&A, 591, A90
Roussel, H. 2013, PASP, 125, 1126
Schisano, E., Rygl, K. L. J., Molinari, S., et al. 2014, ApJ, 791, 27
Schneider, N., Csengeri, T., Bontemps, S., et al. 2010, A&A, 520, A49
Smith, R. J., Glover, S. C. O., & Klessen, R. S. 2014, MNRAS, 445, 2900
Smith, R. J., Glover, S. C. O., Klessen, R. S., & Fuller, G. A. 2016, MNRAS, 455, 3640
Tafalla, M., & Hacar, A. 2015, A&A, 574, A104
Toalá, J. A., Vázquez-Semadeni, E., & Gómez, G. C. 2012, ApJ, 744, 190
Van Loo, S., Keto, E., & Zhang, Q. 2014, ApJ, 789, 37
Vázquez-Semadeni, E., Gómez, G. C., Jappsen, A. K., et al. 2007, ApJ, 657, 870
Vázquez-Semadeni, E., Gómez, G. C., Jappsen, A.-K., Ballesteros-Paredes, J., & Klessen, R. S. 2009, ApJ, 707, 1023
Whitworth, A. P., & Ward-Thompson, D. 2001, ApJ, 547, 317
Zamora-Avilés, M., Vázquez-Semadeni, E., & Colín, P. 2012, ApJ, 751, 77